Supplementary Materials for

A Neural Circuit for Memory Specificity and Generalization

This file includes:

1. Materials and Methods
2. Supplementary Figs. S1 to S13
3. Supplementary References

1. Materials and Methods

Vector construction: Three AAV vectors were constructed. In the mCherry-IRES-Syb2-EGFP vector, the following components were arranged sequentially downstream of left-ITR of AAV2: synapsin promoter, mCherry, IRES, Syb2-EGFP fusion, WPRE, hGH poly A sequence and right ITR. In the WGA-cre AAV vector, the following components were arranged sequentially downstream of left-ITR of AAV2: synapsin promoter, mCherry, IRES, WGA-cre fusion, WPRE, hGH poly A sequence and right ITR. In DFI-TetTox AAV vector, the following components were arranged sequentially downstream of left-ITR of AAV2: CMV promoter and beta-globin intron, loxp2272, loxp, inverted EGFP-2A-TetTox, loxp2272, loxp, hGH poly A sequence and right ITR. Three lentiviral vectors were used. The lentiviral vetor for TetTox was described previously (*S1*). To construct NL2 KD vector, short hairpin sequence containing Nl2 sequence 5'- GCA AGT TCA ACA GCA AGG A-3' was cloned into Xho1-Xba1 locus downstream of the H1 promoter of the control lentiviral vector described previously (*S1*). To make the ChiEF-tdTomoato vector, ChiEF-tdTomoato was subcloned into the locus under the ubiqutin promoter of the FUW vector.

Lentivirus and AAV preparation: Lentivirus were prepared as described (*S2*-*S3*). AAVs were packaged with AAV-DJ capsids for high efficiency *in vivo* neuronal infection. Virus was prepared with a procedure as described (*S4*). Briefly, AAV vectors were co-transfected with pHelper and pRC-DJ into AAV-293 cells. 72 hr later, cells were collected, lysed and loaded onto iodixanol gradient for centrifugation at 400,000g for 2 hrs. The fraction with 40% iodixanol of the gradient was collected, washed and concentrated with 100,000 MWCO tube filter. The infectious titer of virus was measured by infecting HEK293 cells.

Stereotaxic injection: C57BL/6 mice were anesthetized with tribromoethanol (125-250 mg/kg). Viral solution was injected with a glass pipette at a flow rate of 0.15 µl/min. The coordinates used for the prefrontal injection were AP -1.25 mm, ML ±0.3 mm, DV-1.0 mm and -1.5 mm (from dura). The sites at DV-1.0 mm and -1.5 mm both received 1 µl of injection. Coordinates used for N. reuniens injection were AP +1.30 mm, ML 0 mm, DV -4.65 mm. Coordinates used for MD injection were AP +1.35 mm, ML ±0.65 mm, DV -3.5 mm. Coordinates used for striatal injection were AP -0.55 mm, ML ±1.50 mm, DV -3.5 mm. The injections were bilateral except otherwise noted**.**

Optogenetic Implantation and Stimulation: Mice were anesthetized with tribromoethanol (125-250 mg/kg) and the lentiviral vector for expression of channelrhodopsin (ChiEF-tdTomato) was first injected into N. reuniens as described above. 15 min after viral injection, a cannula with optic fiber in the center (mono fiberoptic cannula, 0.2 mm in diameter for the optical fiber) was implanted to target the tip of the optic fiber at the top edge of N. reuniens with the following coordinates: AP +1.30 mm, ML 0 mm, DV -4.25 mm. The cannula was then secured on the skull with dental cement. Behavior experiments were conducted at least 4 weeks after the viral injection and implantation. A 100-mW 473-nm DPSS Laser System was used to generate the 473-nm

blue light for photostimulation. Before each experiment, the output of the laser was measured and adjusted to 20 mW. A flexible optic fiber cable was used to connect the output of the laser to the implanted cannula for intracranial light delivery. The mice were handled daily with all optics connected for 5 consecutive days before the fear conditioning training to reduce anxiety. The onset, frequency and duration of photostimulation were controlled by a programmable stimulator attached to the laser system.

Fear Conditioning: 2 month-old male C57BL/6 mice were housed individually with normal 12/12 hr daylight cycle. They were handled daily for 5 days prior to training. On training day, mice were placed in fear conditioning chamber located in the center of a sound attenuating cubicle. The conditioning chamber was cleaned with 10% ethanol to provide a background odor. A ventilation fan provided a background noise at ~55 dB. After a 2 min exploration period, 3 tone-footshock pairings separated by 1 min intervals were delivered. The 85 dB 2 kHz tone lasted for 30 s and the footshocks were 0.75 mA and lasted for 2 s. The foot shocks co-terminated with the tone. The mice remained in training chamber for another 30 seconds before being returned to home cages. In context test, mice were placed back into the original conditioning chamber for 5 min. During altered context test, the conditioning chamber were modified by changing its metal grid floor to a plastic sheet, white metal side walls to plastic walls decorated with red stripes, background odor of ethanol to vanilla. The ventilation fan was turned off to reduce background noise. Mice were placed in the altered chamber for 5 min to measure the freeze level in the altered context and after this 5-min period a tone (85 dB, 2 kHz) was delivered for 1 min to measure the freeze to tone. The behavior of the mice was recorded with the Freezeframe software and analyzed with Freezeview software. Motionless bouts lasting more than 1 second were considered as freeze. Animal experiments were conducted following protocols approved by Administrative Panel on Laboratory Animal Care at Stanford University.

Histology and immunohistochemistry: Mice were anesthetized with tribromo-ethanol and perfused with 10 ml of PBS followed by 50 ml of fixative (4% paraformaldehyde diluted in PBS). The brains were removed and post-fixed for 3 hours at room temperature and then immersed in 30% sucrose solution overnight before being sectioned at 30 μm-thicknesses on a cryostat. The free-floating brain sections were collected in PBS. The sections were counterstained with DAPI and mounted onto glass slides with Vectashield mounting medium. For immunohistochemistry of C-Fos, the brain sections were incubated in blocking solution containing 10% house serum, 0.2% bovine serum albumin and 0.5% Triton X-100 for 1 h and then incubated with the primary antibodies for c-Fos (rabbit, calbiochem, 1:2000 dilution) and for NeuN (mouse, Millipore, 1:1000 dilution) overnight at room temperature. After washing, the sections were incubated with florescent second antibodies for 2 h (1:500 dilutions). After extensive washing, the sections were mounted onto glass slides with Vectashield mounting medium.

Quantification of mRNA level by qRT-PCR. The cultured cortical neurons were lysed and total RNA was extracted and purified with RNAqueous-Micro kit following the manufacturer's instructions. The mRNA level of individual genes was then analyzed by one-step quantitative RT-PCR system with pre-madeTaqMan gene expression assays. Briefly, 30 ng of RNA sample in 1 µl volume was mixed with 10 µl of TaqMan fast universal PCR master mix (2x), 0.1 µl of reverse transcriptase **(**50 units/µl), 0.4 ul of RNase inhibitor (20 units/µL), 7.5 µl of H_2O and 7 µl of TaqMan gene expression assay for the target gene (including the forward and reverse primers and the TaqMan FAM-MGB probe). The reaction mixture was loaded onto ABI7900 fast RT-PCR machine for 30 min of reverse transcription at 48 °C followed by 40 PCR amplification cycles consisting of denaturation at 95°C for 1 s, annealing and extension at 60 °C for 20 s. The amplification curve was collected and analyzed with ΔΔCt methods for relative quantification of mRNAs. The amount of mRNA of target genes, normalized to that of an endogenous control and relative to the calibrator sample is calculated by $2^{-\Delta\Delta Ct}$. In the current study, glyceraldehyde 3-phosphate dehydrogenase (GAPDH) was used as the endogenous control and the RNA samples derived from neurons infected with control vector was used as the calibrator.

Brain Slice Electrophysiology: 2-month old C57BL/6 mice were injected with control lentivirus or NL2 KD lentivirus and were used for slice physiology at least 2 weeks after the infection. Coronal brain slices slices (300 µm) were cut with a vibratome in ice cold solution comprising (in mM): 75 Sucrose, 85 NaCl, 2.5 KCl, 1.3 NaH2PO4, 4 MgSO4, 0.5 CaCl2, 24 NaHCO3, 25 D-glucose saturated with 95% O_2/5% CO_2 and transferred to a holding chamber containing artificial cerebrospinal fluid (ACSF) composed of (in mM): 126 NaCl, 2.5 KCl, 1 NaH2PO4, 1.3 MgSO4, 2.5 CaCl2, 26.2 NaHCO3, 11 D-glucose to recover for half an hour at 31 ^oC and followed by at least one hour recovery at room temperature before being transferred to a recording chamber continually perfused (1 ml/min) with oxygenated ACSF (maintained at 26-28^oC) containing 20 µM of CNQX, 50 µM of APV and 1 µM of tetrodotoxin. Whole-cell voltage-clamp recordings were made with 2.3-3 MΩ pipettes filled with internal solution containing (in mM): 135 CsCl, 10 HEPES, 1 EGTA, 1 Na-GTP, 4 Mg-ATP. Neurons were clamped at -70 mV for recording of mIPSCs.

2. Supplementary Figures and Figure Legends

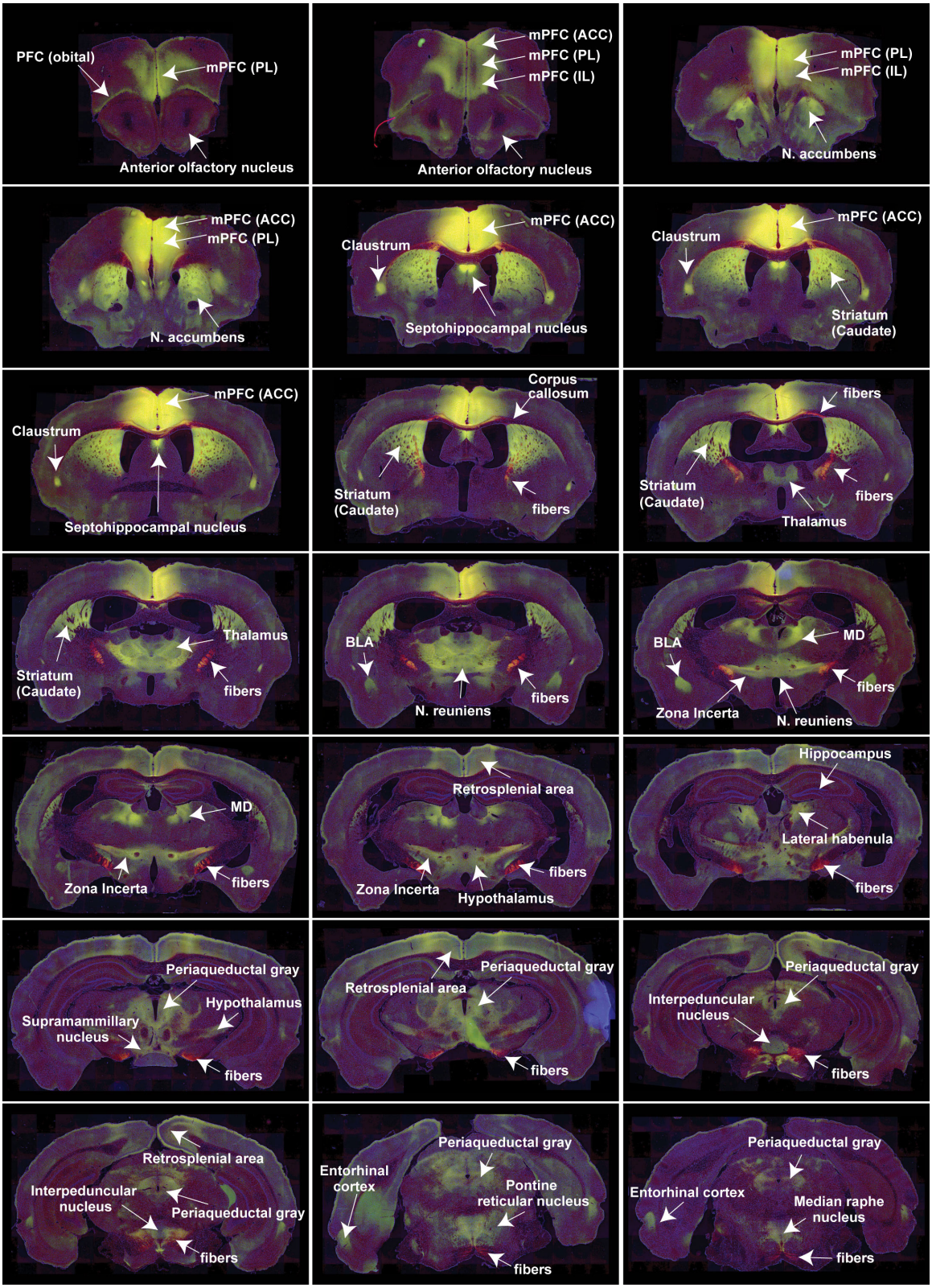

Fig. S1

Synaptic outputs of mPFC neurons (related to Fig. 1)

Mice (2 months old) were stereotactically injected with SynaptoTag-AAVs into the medial prefrontal cortex (mPFC) primarily targeting the anterior cingulate cortex [ACC]; Figure 1B). Mice were sacrified eight weeks after injections, and coronal sections were analyzed by fluorescence microscopy for the expressed EGFP (green; EGFP is fused to synaptobrevin/VAMP and thus is specific for presynaptic nerve terminals at synapses), and mCherry (red; fills the entire neuron). Data shown are representative images obtained from a single mouse at different coronal section levels. Green fluorescence indicates the locations of synaptic terminals formed by the infected mPFC neurons. The intensity and density of green puncta reflect the strength of synaptic connectiions. Red fluorescence indicates the somata of infected mPFC neurons and their axonal projections; the somata of the mPFC neurons appear yellow at this magnification due to overlapping green fluorescence provided by abundant synapses formed by mPFC neurons within the mPFC. mCherry-positive neurons are located in the three major sub-regions of the mPFC, the infralimbic cortex (IL), the prelimbic cortex (PL), and the anterior cingulate cortex (ACC). Note that mCherry-positive axonal fibers form a prominent axonal bundle labeled red that passes through the corpus callosum, the dorsal striatum, the dorsal thalamus, the hypothalamus and the midbrain structures. Among brain regions outside of the mPFC receiving a high level of synaptic inputs from the mPFC are the septohippocampal nucleus of the lateral septum complex, the nucleus accumbens, the mediodorsal striatum, the mediodorsal nucleus of the thalamus (MD), the midline thalamus (mainly N. reuniens), the zona incerta, the claustrum, hypothalamic nuclei, basolateral amygdala, and the midbrain periaqueductal gray. Within the cortex, the mPFC projects laterally to surrounding cortical areas and forms dense synaptic connections in layer 1.

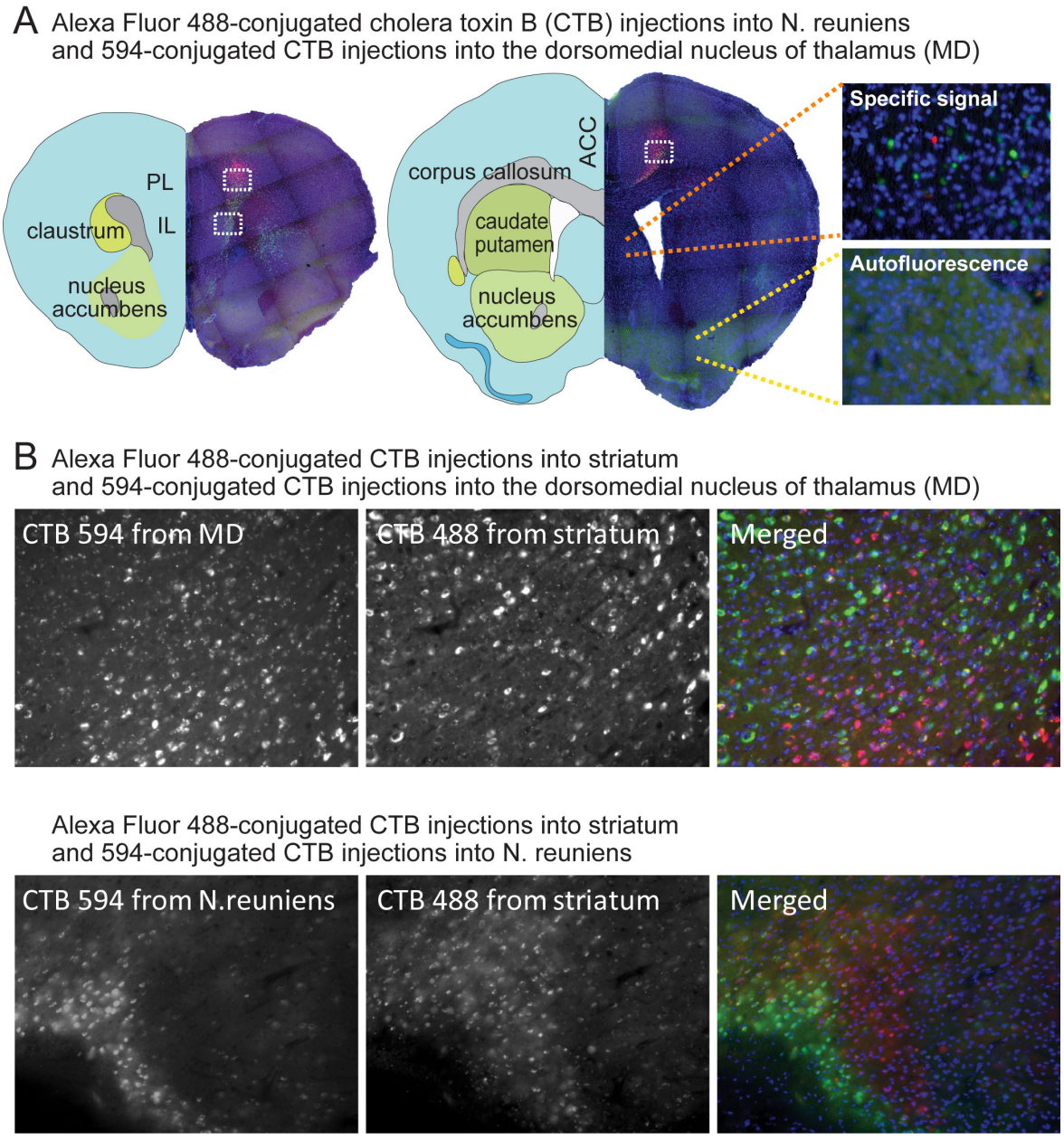

Fig. S2

Retrograde tracing of mPFC neurons from different brain regions using cholera toxin-B (CTB) injections (related to Fig. 1)

A. Low magnification images showing the distribution of neurons traced by CTB injections into the N. reuniens (CTB-488; green) or the mediodorsal nucleus of thalamus (MD; CTB-594, red). Fluorescently tagged CTB's were stereotactically injected into the in indicated brain regions into 2 month old mice. Mice were sacrificed and analyzed by fluorescence microscopy after two weeks. The neurons connected with the N. reuniens were more abundant in the infralimbic mPFC (IL), while neurons connected with the MD were more abundant in the prelimbic (PL) and anterior cingulate cortex (ACC) regions of the mPFC. Dashed boxes indicate the locations of origin for the high-resolution images shown in Figure 1B. Please note that brain sections exhibit weak green autofluorescence, which is apparent in the basal brain areas on the photos shown here. The high magnification photos on the right are the enlargements of the two indicated brain regions

demonstrating the difference between autofluorescence and the specific fluorescence signal of the tracers.

B. Representative images of the mPFC (ACC region) showing neurons traced by CTB injections into either the mediodorsal thalamic nucleus (MD) and the medial dorsal striatum (upper panels), or the N. reuniens and the medial dorsal striatum (lower panel). Note the segregation between mPFC neurons projecting to different target areas.

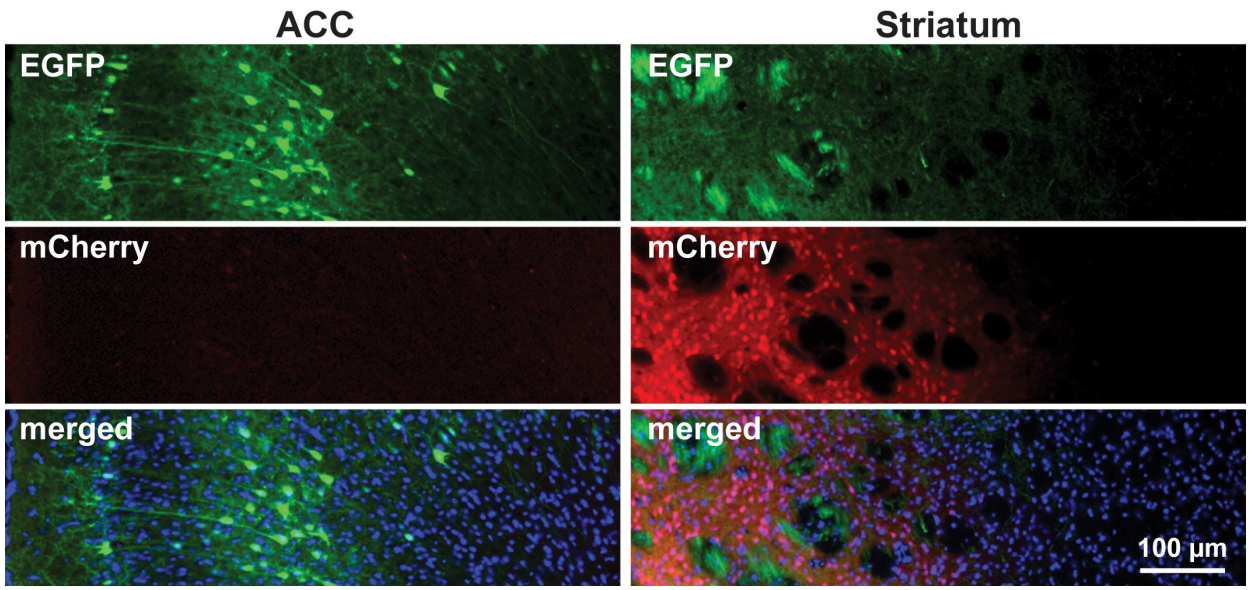

Fig. S3

Retrograde cre-dependent tracing of mPFC projection neurons by WGA-cre expressed in the dorsomedial striatum, demonstrating retrograde introduction of active cre recombinase (which then activates EGFP and TetTox expression) specifically into mPFC neurons projecting to the striatum (related to Fig. 2)

High-magnification views of the anterior cingulate cortex (ACC) and the dorsomedial striatum obtained from the brain section shown in Figure 2B. WGA-cre AAVs were stereotactically injected into the striatum, and double-floxed EGFP-TetTox AAV into the mPFC to map projections from the striatum to the mPFC. EGFP expression in the ACC identifies neurons receiving WGA-cre from their striatal projection targets. Mice were injected at 2 months of age, and analyzed 4 weeks after injections. EGFP expression in the striatum indicates the distribution of axons and presynaptic terminals arising from the EGFP-positive mPFC neurons that were activated by retrogradely transported WGA-cre. mCherry expression denotes striatal neurons expressing WGA-cre. The fact that mCherry is absent from the mPFC demonstrates that the mCherry are not retrogradely transported, but only the WGA-cre that is produced by infected striatal neurons. In the striatum, EGFP-positive fibers and terminals were largely limited to the regions with mCherry-positive neurons, indicating that the mPFC neurons with EGFP expression selectively projected to the region where WGA-cre was expressed.

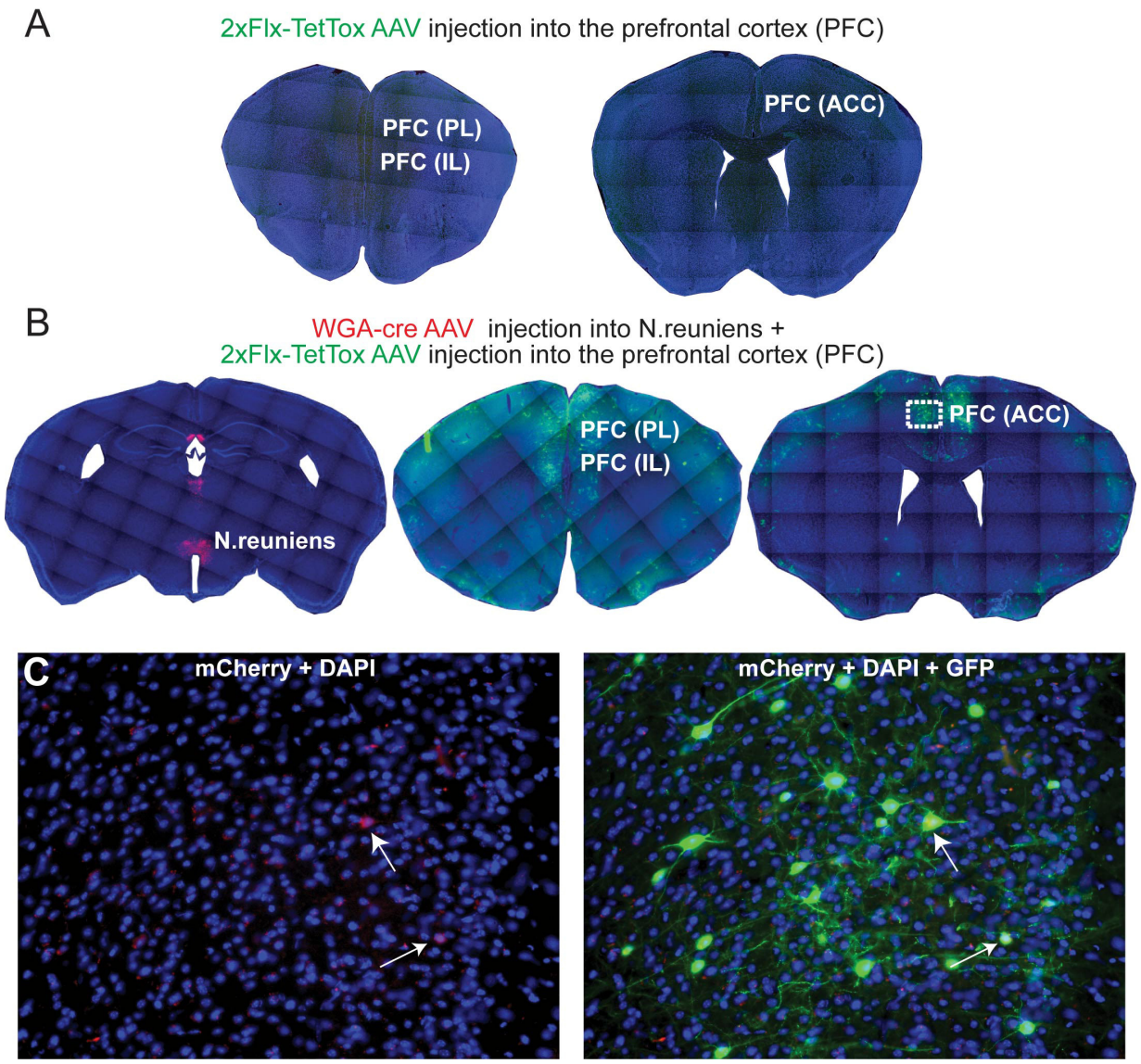

Fig. S4

Retrograde cre-dependent tracing of mPFC projection neurons by WGA-cre expressed in the N. reuniens, demonstrating retrograde introduction of active cre recombinase (which then activates EGFP and TetTox expression) specifically into mPFC neurons projecting to the striatum (related to Fig. 2)

A. Coronal brain sections from a mouse that was stereotactically injected with 2xFlx-TetTox-EGFP AAV in the mPFC, but not with WGA-cre AAV. Mice (2 months old) were stereotactically injected with 2xFlx-TetTox-EGFP AAV in the mPFC and were analyzed eight weeks after injections. Coronal sections were examined by fluorescence microscopy for the expression of EGFP and mCherry. Without co-injection of WGA-cre AAV into brain regions connected with the mPFC, no GFP or mCherry fluorescence could be detected.

B. Coronal brain sections from a mouse that was stereotactically injected with 2xFlx-TetTox-EGFP AAV in the mPFC, and with WGA-cre AAV in the N. reuniens. Red fluorescence indicates expression of mCherry from the WGA-cre AAV, and green fluorescence expression of EGFP and TetTox in the mPFC that is activated by trans-neuronal retrograde transport of WGA-cre from the N. reuniens. Note that most of the apparent green fluorescence at the edges of the brain sections

is due to autofluorescence which does not represent individual neurons as examined in high-magnification images.

C. Enlargement of the boxed area in the ACC section in (B), depicting mPFC neurons with EGFP expression that is activated by WGA-cre transported from the N. reuniens. Arrows point to EGFP-positive neurons which also express mCherry in the soma, indicating that only a very small fraction of mPFC neurons received retrogradely transported AAV vectors (please note that the small red dots were axons from the mcherry-expressing N. reuniens neurons).

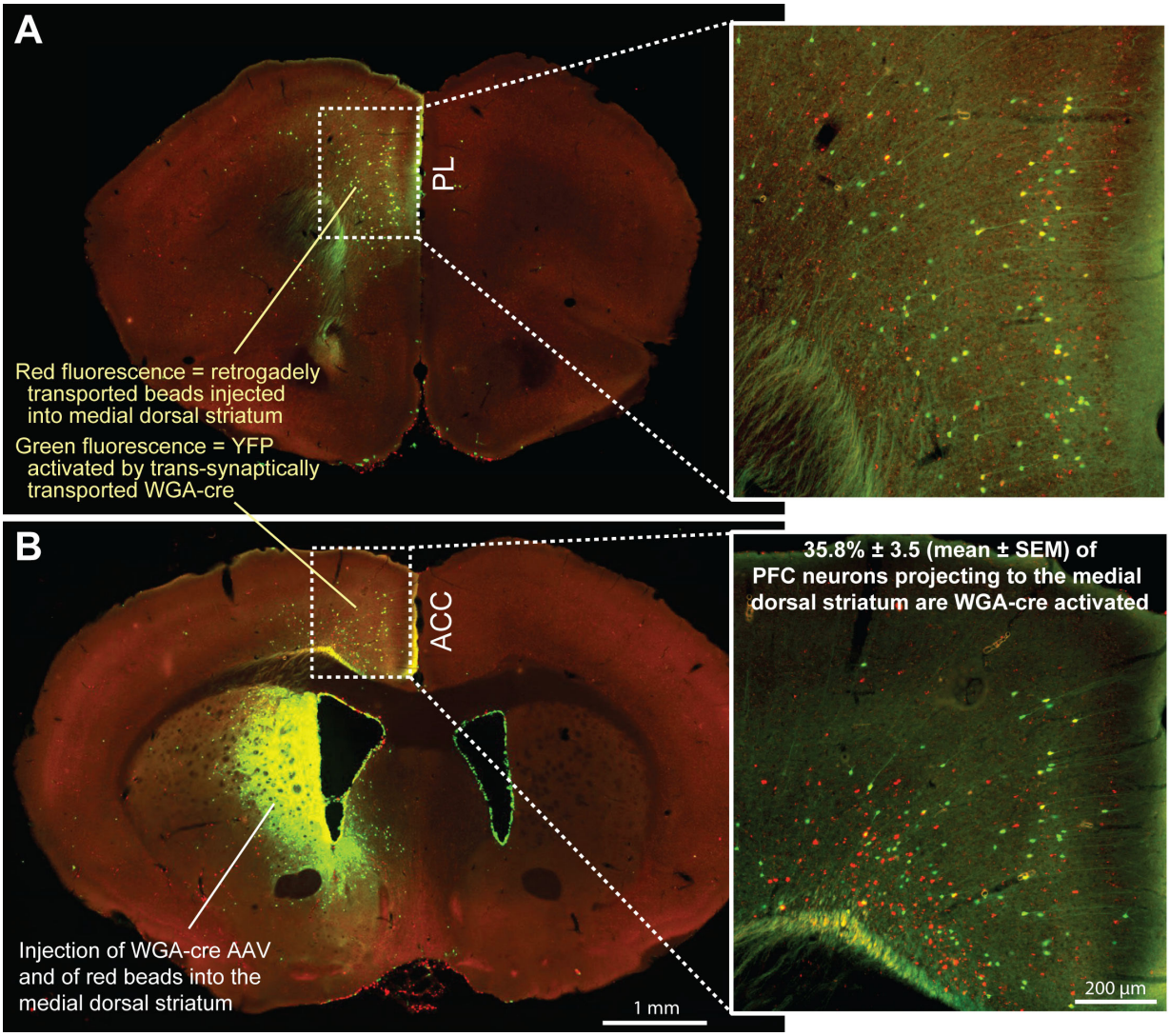

Fig. S5

Determination of the efficiency of retrograde cre-dependent tracing of mPFC projection neurons by WGA-cre expressed in the dorsal striatum (related to Fig. 2)

A and **B.** Images of representative coronal brain sections at two levels from a EYFP reporter mouse (Ai3 mouse) that was stereotacticallly injected with WGA-cre AAVs and red tracer beads into the medial dorsal striatum (a mixture of 0.3 µl of AAV and 0.2 µl of beads, indicated in B). Ai3 Mice (The Jackson laboratory, Stock Number: 007903) carry a loxP-flanked STOP cassette preventing transcription of a CAG promoter-driven enhanced yellow fluorescent protein (EYFP). EYFP is only expressed following Cre-mediated recombination. The mice were injected at 2 months of age, and analyzed 4 weeks later by fluorescence microscopy. Images on the right depict enlargements of the areas that are boxed in the images on the left; scale bars on the bottom apply to both images on the left and right, respectively (ACC, anterior cingulate cortex; PL, prelimbic cortex). The number of red and green neurons in the ACC were counted in three independently injected mice, and the percentage of green WGA-cre activated neurons as a function of the total number of red projection neurons was determined (35±3.5%; n=3). Note that the vast majority of mPFC neurons project only ipsilaterally.

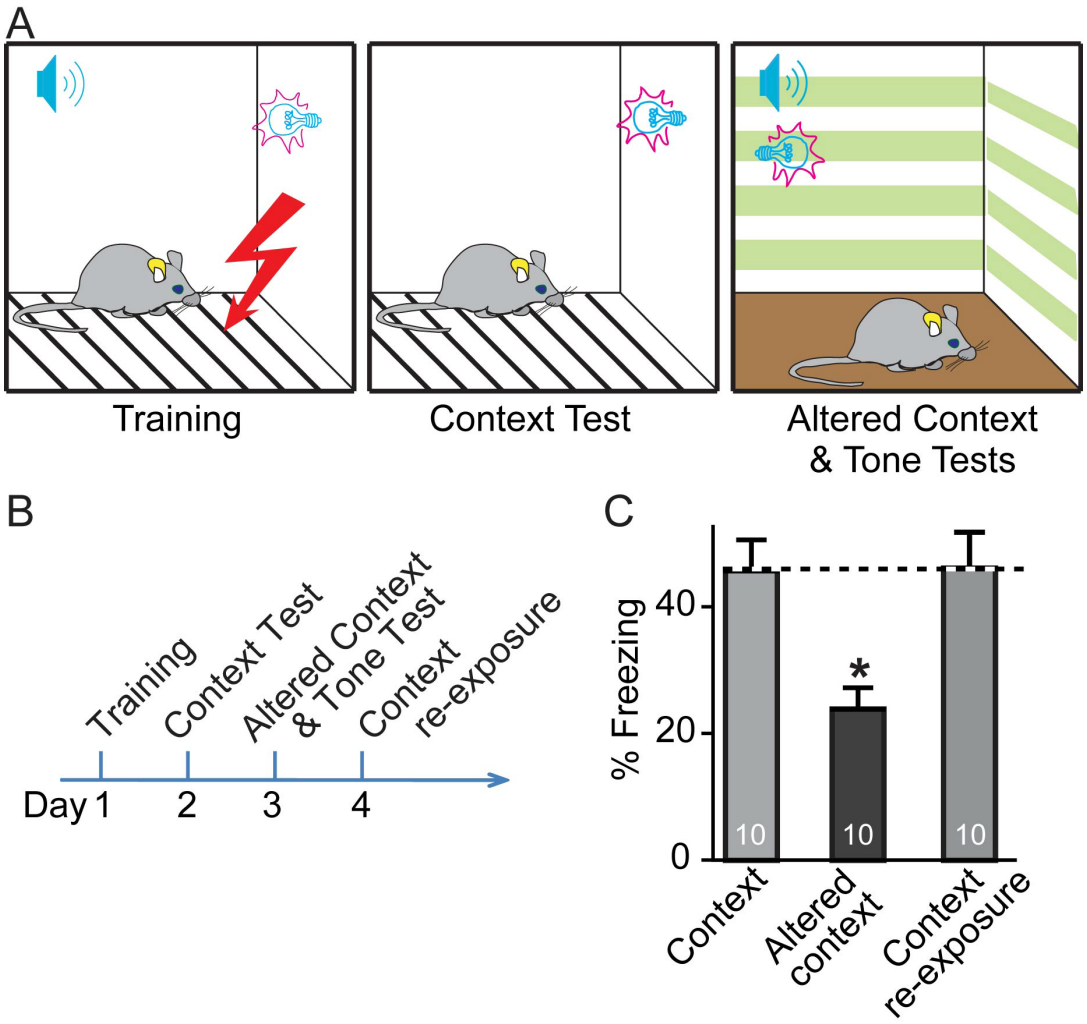

Fig. S6

Fear conditioning tests (related to Fig. 2)

A. Illustration of the experimental conditions for fear conditioning training and tests. The altered context differs from the training context in the floor and wall design, background odors, ambient noise, and location of light source. A more detailed description is available in the "**Materials and Methods"**.

B. Schematic diagram of the experimental protocol.

C. Naïve mice show reduced freezing in the altered context, indicating that mice treat the altered context as different from the training context. The different responses were not due to extinction of fear memory since the freezing level returned if the mice were re-exposed to the training context after the altered context tests. Data are means ± SEM; n=10 mice. Statistical significance was assessed by one-way ANOVA followed by Turkey's post-hoc test (* $P<0.05$).

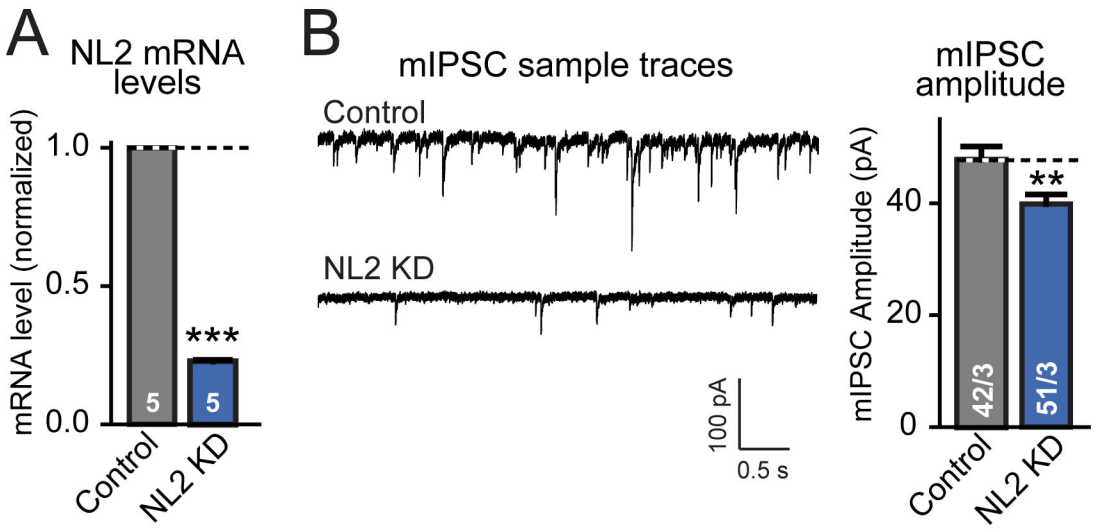

Fig. S7

Efficiency of the neuroligin-2 knockdown (NL2 KD), and effect of in vivo neuroligin-2 knockdown on inhibitory inputs into the N. reuniens (related to Fig. 3)

A. Cultured cortical neurons were infected with a control (only expressing EGFP) or NL2 KD lentivirus at DIV6 and collected for quantitative RT-PCR to measure NL2 mRNA level at DIV14. Data are means ± SEMs. The numbers inside the columns indicate the batches of cultures analyzed.

B. NL2 KD dramatically decreases inhibitory inputs into the N. reuniens. Patch-clamp recordings from acute N. reuniens slices obtained from mice that were stereotactically injected with control of TetTox expressing lentivirus into the N. reuniens. Mice were injected at 2 months of age, and analyzed two weeks later. The number of neurons/mice analyzed are indicated in the bar diagram.

Statistical significance between the two groups was calculated by Student's t-test (2-tailed). **, $p<0.01$; ***, $p<0.001$.

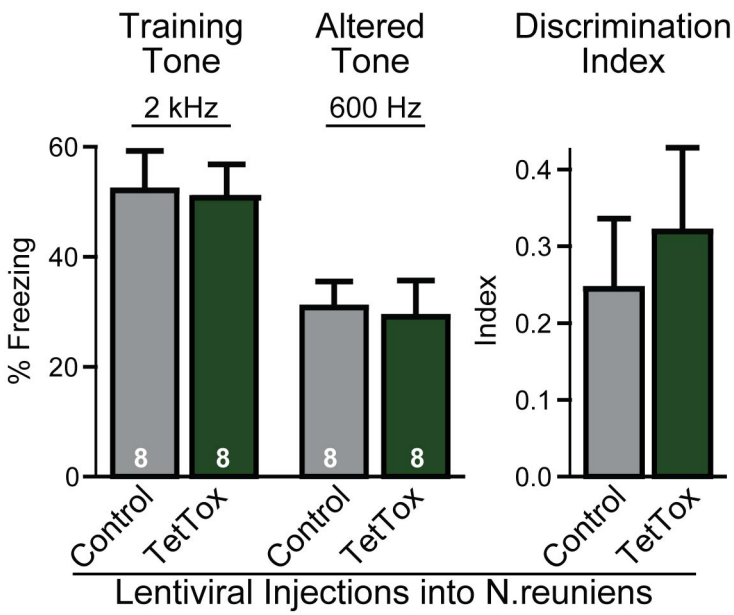

Fig. S8

Generalization of cued memory is not impaired by TetTox-mediated silencing of N. reuniens neurons (related to Fig. 3).

Mice were stereotactically injected in the N. reuniens with control lentivirus or TetTox expressing lentivirus, and then trained for cued fear conditioning. The mice received 3 tone-footshocks pairings separated by 2 min intervals. The 85 dB 2 kHz tone was used as conditional stimulus which lasted for 30 s and co-terminated with a footshock (0.75 mA, 2 s). Between each of two consecutive tone-footshock pairings, a 75 dB 600 Hz tone was presented without footshock delivered. On the second and the third day after training, the mice were tested for freezing to the 2 KHz tone and to the 600 Hz tone. The bars graphs on the left show the freezing levels to the two tones, and the bar graph on the right depicts the discrimination index (the difference between freezing to 2 kHz tone and freezing to the 600 Hz tone, divided by the sum of freezing to both). No statistically significant difference between control mice and mice expressing TetTox in the N. reuniens was noted. Data are means ± SEM; n=8 mice.

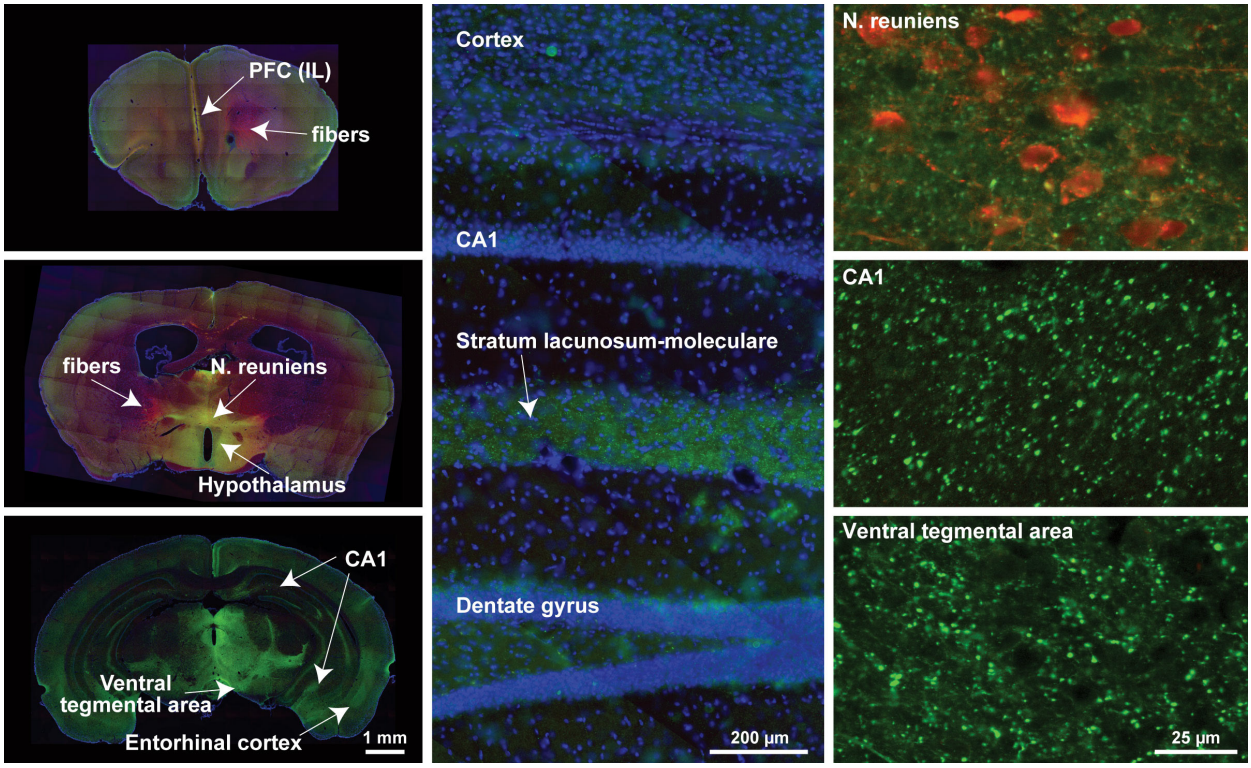

Fig. S9

SynaptoTag-AAV mapping of synaptic projections from the N. reuniens (related to Figs. 3 and 5)

SynaptoTag AAV (Fig. 1A) was stereotactically injected into the N. reuniens of 2 month-old mice, and the localization of EGFP and mCherry was imaged by double immunofluorescence labeling 8 weeks later (see Fig. S1 for an explanation of the technology). Data show representative low- (left panels), middle- (middle panel) and high-magnification images (right panels) of coronal sections obtained from a single representative mouse, but independently reproduced multiple times. N. reuniens neurons form direct synaptic connections with several target regions, including the hypothalamus, the CA1 region of the hippocampus, layer 1 of the mPFC, the ventral tegmental area, and the entorhinal cortex. The middle panel depicts an enlargement of CA1 region showing that the inputs from N. reuniens to the hippocampus (green; red = DAPI staining) are restricted to the stratum lacunosum-moleculare, where these terminals form synapses on the distal apical dendrites of CA1 pyramidal cells together with the synaptic terminals from the entorhinal cortex. The high-magnification views (right panels) reveal a punctate distribution of the synaptic labeling or axonal projections from N. reuniens neurons throughout two selected target regions (the stratum lacunosum-moleculare of the CA1 region of the hippocampus, and the ventral tegmental area), but similar labeling is observed in other target regions.

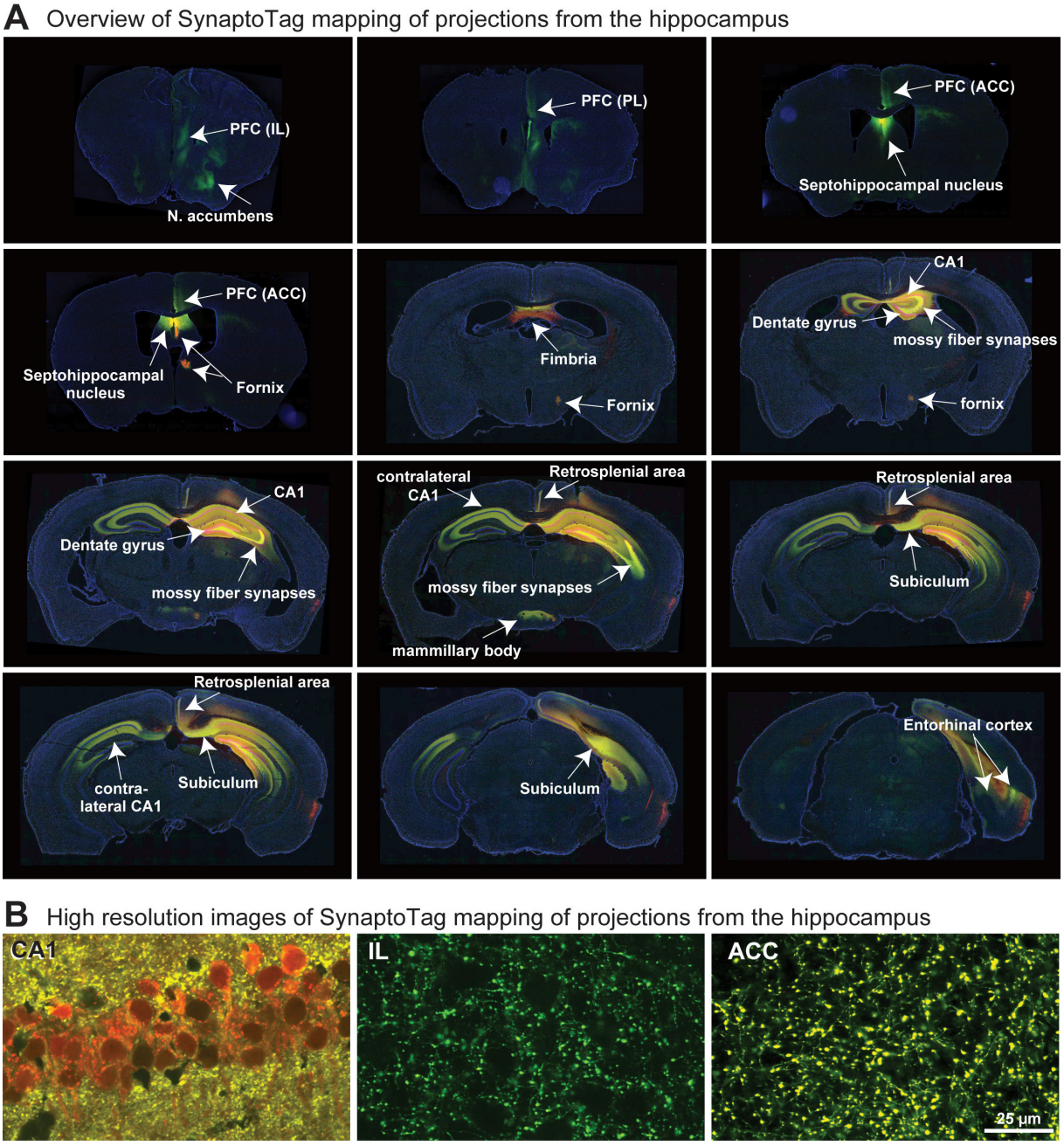

Fig. S10

SynaptoTag-AAV mapping of synaptic projections from the hippocampus (related to Figs. 3 and 5).

A. SynaptoTag AAV (see Fig. S1A) was stereotactically and unilaterally injected into the CA1-region and dentate gyrus of the hippocampus of 2-month old mice. Mice were sacrificed 8 weeks later, and the localizations of mCherry (labeling the entire cytoplasm) and EGFP (labeling only presynaptic terminals) were imaged in coronal sections by their intrinsic fluorescence. Note that the hippocampal neurons formed the majority of their synapses with neurons in the contralateral hippopcampus, the subiculum, the entorhinal cortex, the mPFC, the retrosplenial area and the septohippocampal nucleus. In the retrosplenial area, the synapses were specifically located in layer 2. Axons arising from the hippocampus formed the fornix which reached the mamillary body

and established synaptic connections there. The hippocampus forms direct synaptic connections with all three major subregions of the mPFC: the Infralimbic cortex (IL), the prelimbic cortex (PL) and the anterior cingulate cortex (ACC).

B. High resolution images showing synapses formed by hippocampal neurons. The red fluorescence in CA1 indicates mCherry-expressing neurons. The green fluorescence in CA1, IL or ACC depicts the synaptic terminals derived from infected hippocampal neurons.

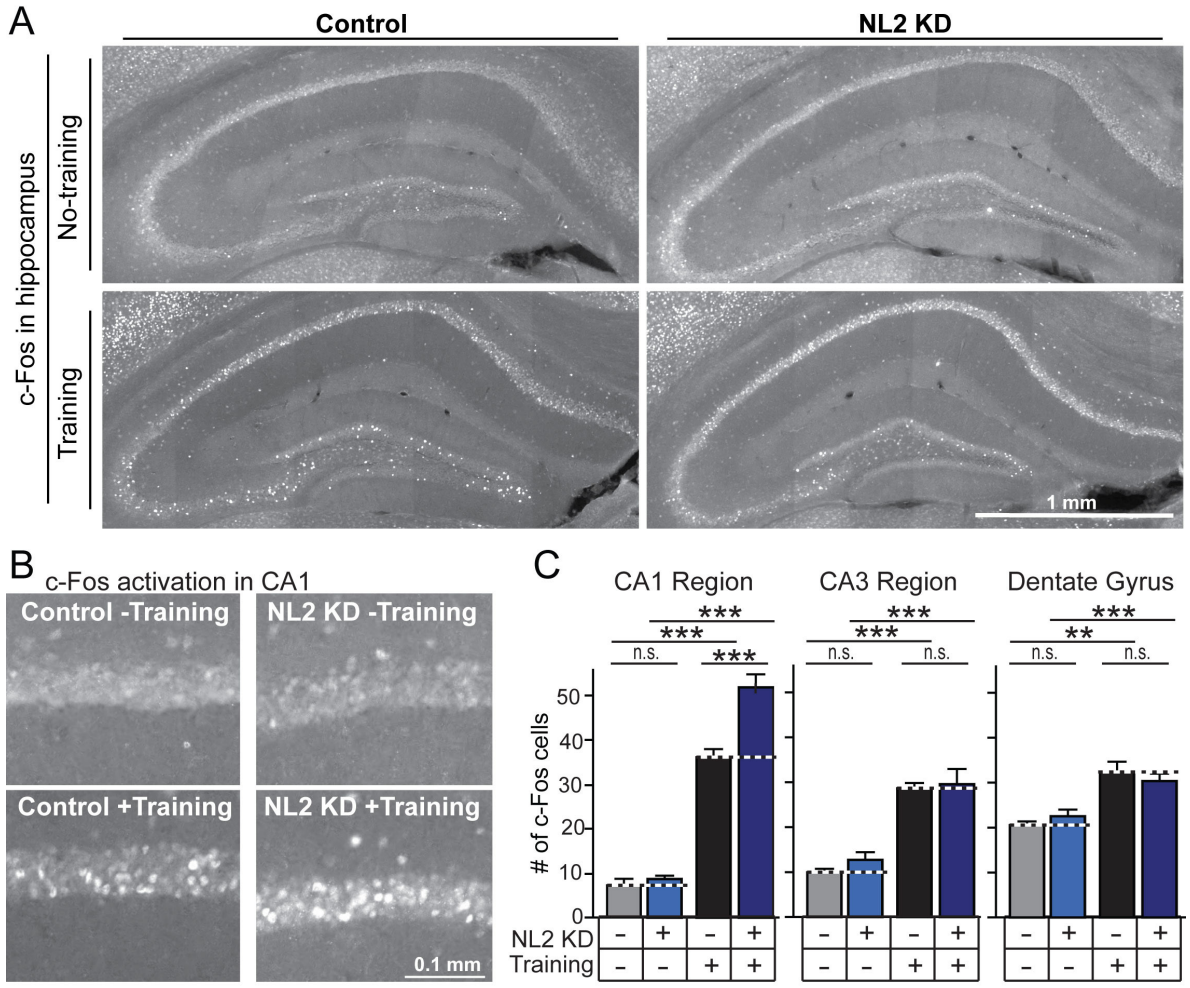

Fig. S11

Eploratory experiment to measure the effect of the neuroligin-2 knockdown (NL2 KD) in the N. reuniens on the activation of neurons by fear conditioning training in the hippocampus (initial experiments in preparation to those described in Figs. 3 and S12)

A, Representative images of c-Fos immunoreactive neurons in the hippocampus from control mice or mice in which NL2 KD shRNAs were expressed in the N. reuniens, with or without fear conditioning training. Sections were stained with antibodies to c-Fos and with a nuclear dye (DAPI).

B and **C**, Quantification of the effect of fear conditioning training, with or without knockdown of neuroligin-2 in the N. reuniens, on the activation of neurons in the hippocampus. Neuronal activation was measured by c-Fos expression. Control or the neuroligin-2 knockdown (NL2 KD) lentiviruses were injected into the N. reuniens of adult mice which were then subjected to control or fear conditioning training. Brains were fixed 90 min after training, and c-Fos immunoreactivity in the hippocampus was measured by immunocytochemistry (Panel B, representative high-resolution images of the CA1 region of the hippocampus; Panel C, quanitation of c-Fos immunoreactive neurons per section in the three major hippocampal areas). Data shown are means ± SEMs; n = 16-20 sections from 4 mice in each group. Statistical significance was assessed by two-way ANOVA followed by Bonferroni's post-hoc test (** P<0.01; *** P<0.001).

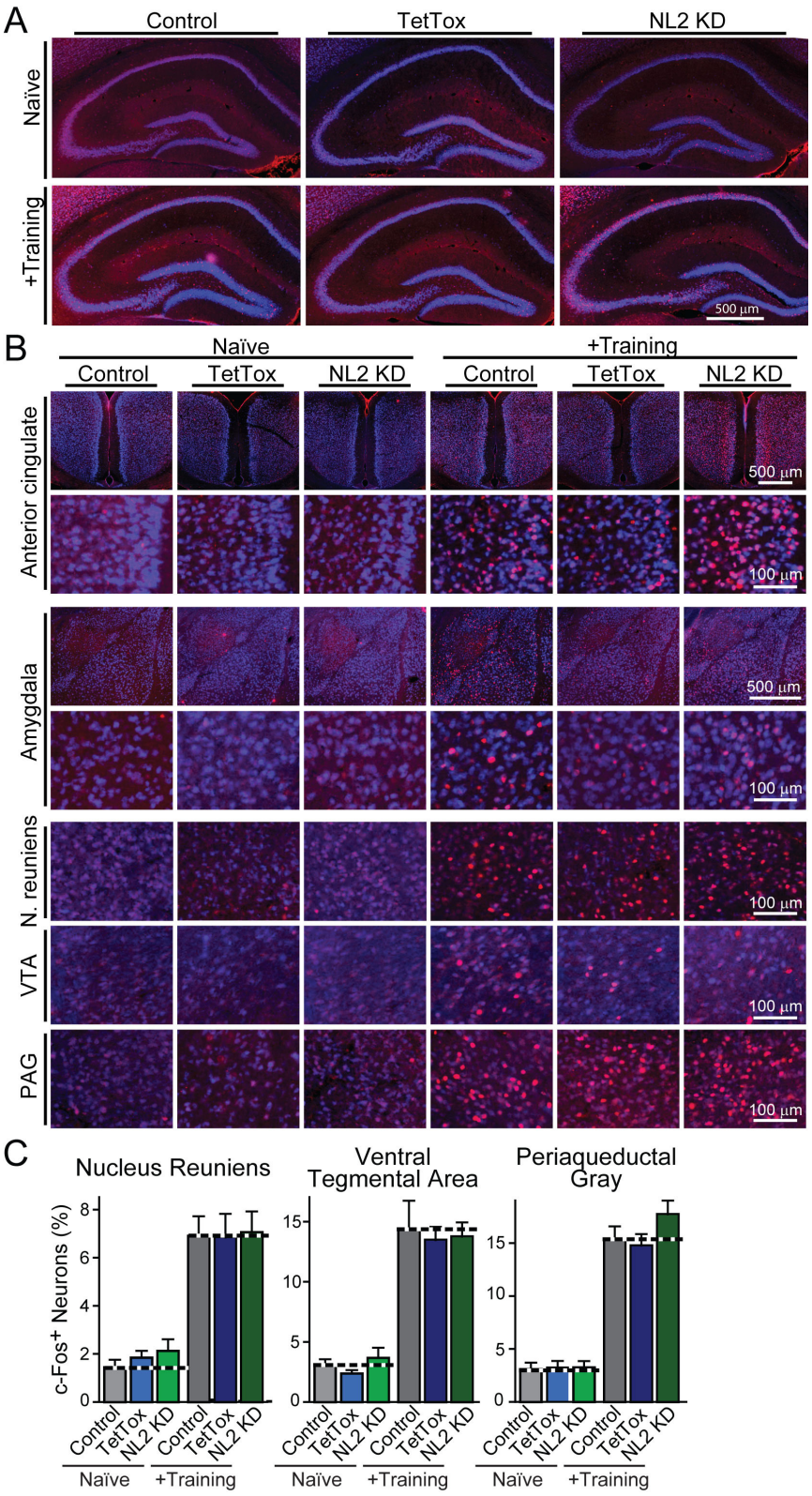

Calibration bars on the right apply to all panels in a row.

Fig. S12

Effect of training during fear conditio-ning, combined with TetTox expression or neuroligin-2 knockdown in the N. reuniens, on neuronal activation in different target brain regions (related to Fig. 3)

Control lentivirus, Tet-Tox lentivirus, or the neuroligin-2 knock-down (NL2 KD) lentivirus was injected into the N. reuniens of adult mice. Mice were subjected to fear conditioning training ('+training') or were not subject to training ('naïve'). The mice were sacrificed 90 min after training, and c-Fos immunoreac-tivity was measured by immuno-cytochemistry in various brain areas.

A, Representative low-power images of the hippocampus stained for c-Fos (red) and neuronal nuclei (NeuN; blue) under the six conditions of the experiments. Calibration bar applies to all panels.

B, Representative high-resolution images of the five non-hippocampal brain regions examined for neuronal activation under the six conditions of the experiment. Staining was performed for c-Fos as a measure of neuronal activation (red) and for NeuN to label all neuronal nuclei (blue).

C, Quanitation of c-Fos immunoreactive neurons per total neurons in the indicated brain areas. These are additional quantifications to complement thos sown in Fig. 3I. Data shown are means ± SEMs; n = 12-18 sections from 4 mice in each group. Statistical significance was assessed by two-way ANOVA followed by Bonferroni's post-hoc test. There is no significance difference between the three N. reuniens treatment conditions (control, TetTox, and NL2 KD) in the naïve and trained sets, but in all brain regions tested the trained groups exhibit a highly significant ($P<0.001$) increase in the number of activated neurons.

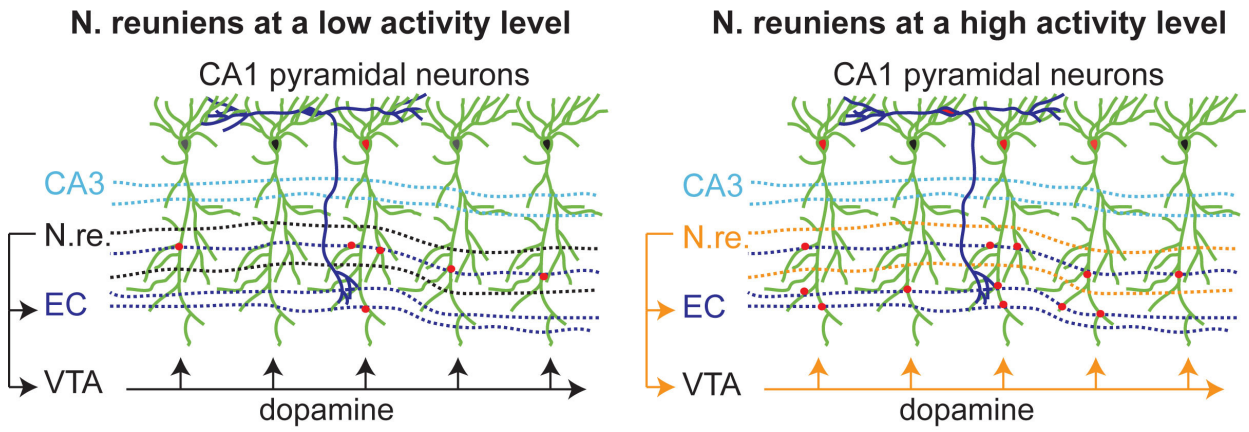

Fig. S13

A model for the hippocampal circuitry underlying the control of memory specificity (related to Fig. 5)

As illustrated in Fig. 5, memories are composed of a combination of features and attributes – but the features are not equally incorporated into memories. The more prominent a feature is, the more likely it is included in a memory. Memories with only the most prominent features have a high probability of overlap with similar items and are generalized memories. When the less prominent features are included in memories, the memories become more specific. It is generally thought that the hippocampus may be responsible for combining and representing the associations of sensory features in brain (*S5-S6*). Synaptic activity carrying the information of "less prominent" features may be too weak to trigger synaptic plasticity and/or neuronal firing in the hippocampus, which will exclude these features from memory representation and storage. N. reuniens neurons directly synapse onto CA1 neurons in the str. moleculare-lacunosum (Fig. S9), and indirectly activate CA1 neurons via their inputs onto EC (entorhinal cortex) or to VTA (ventral tegmental area). Using these connections, the activity level of N. reuniens neurons regulates the neuronal activity and synaptic plasticity in the hippocampus. For example, the "cooperativity" between the N. reuniens-CA1 synapses and the EC-CA1 synapses can reduce the threshold for synaptic plasticity to occur at EC-CA1 synapses (*S7*), which is believed to carry the multimodal sensory information to the hippocampus for memory representation and storage. The ease of synaptic plasticity will therefore allow more less-prominent features to be incorporated into memory, which in turn makes memory more specific. The indirect input from the N. reuniens to CA1 through EC or VTA may exert similar effects through elevating the activity level of the EC neurons or through triggering the release of dopamine in the hippocampus, which will also reduce the threshold for synaptic plasticity (*S8-S9*).

Early modeling studies of the hippocampus proposed the idea of "pattern separation". According to these models, the neurons in the dentate gyrus substantially outnumber their input neurons in the entorhinal cortex. Therefore the activation of dentate gyrus neurons is sparse during memory representation. These sparse representations may have less chance to overlap with each other, and thus allow better "separation" of patterns (*S10*). This "fewer neurons for more specific memories" concept at first glance seems contradictory to the idea of neuronal ensemble activation

that is controlled by the N. reuniens as proposed here. In the following, however, we would like to discuss why we think that our proposal is not at odds with these models.

First, “pattern separation” (and the related “pattern completion”) is primarily a retrieval-based mechanism, while we show in our study that the mPFC-N. reuniens pathway functions during memory acquisition (Figs. 3D-3G). Memories with enriched information can still be subject to the “pattern separation” mechanism when they are retrieved. The enriched information may not necessarily lead to an increased recruitment of dentate gyrus neurons, and it is possible that the enriched information can help to generate an even more sparse activation of dentate neurons. In fact, in monitoring the c-Fos expression, we did not observe alterations in the dentate gyrus when more CA1 neurons become activated (Fig. 3I).

Second, hippocampus-dependent memories are not hard-wired for behavioral responses. Instead, they are expressed as a representation of the memorized material. The behavioral responses are the consequence of a cognitive decision making process, which is likely a cortical function that involves the mPFC. For this purpose, memory representation will need to provide as detailed information as possible for an accurate judgment to be made in the cortex, and more detailed information will likely require participation of more neurons. Moreover, in a pioneering study it has been shown that individual animals show different levels of generalization that inversely correlate with the activity levels of the hippocampus (*S11*). This also argues against the idea that specific memories are generally encoded by few neurons, although they may be sparsely encoded in a particular brain region such as the dentate gyrus for the specific purpose of pattern separation.

Third, the early model of “pattern separation” has met some difficulty in dealing with the results of recent experiments. To reconcile the discrepancy between the model and the experimental data, Gage and colleagues proposed the idea of “memory resolution” which was also built on the notion that more detailed information will make memories more precise (*S12*).

Although understanding the precise coding patterns for memory representation requires much additional study, it seems clear that different circuits (e.g. the entorhinal cortex-dentate gyrus-CA3 circuit vs. the mPFC-N. reuniens-CA1 circuit) utilize different mechanisms, which is also in agreement with our previous observation that different circuits require different types of spike patterns (*S1*).

3. Supplementary References

S1. W. Xu *et al.*, *Neuron* **73**, 990 (Mar 8, 2012).
S2. A. Maximov, Z. P. Pang, D. G. Tervo, T. C. Südhof, *J Neurosci Methods* **161**, 75 (Mar 30, 2007).
S3. Z. P. Pang, P. Cao, W. Xu, T. C. Sudhof, *J Neurosci* **30**, 4132 (Mar 17, 2010).
S4. S. Zolotukhin *et al.*, *Gene Ther* **6**, 973 (Jun, 1999).
S5. H. Eichenbaum, *Neuron* **44**, 109 (Sep 30, 2004).
S6. X. Liu *et al.*, *Nature* **484**, 381 (Apr 19, 2012).
S7. T. V. Bliss, G. L. Collingridge, *Nature* **361**, 31 (Jan 7, 1993).
S8. S. Li, W. K. Cullen, R. Anwyl, M. J. Rowan, *Nat Neurosci* **6**, 526 (May, 2003).
S9. J. E. Lisman, H. J. Pi, Y. Zhang, N. A. Otmakhova, *Biol Psychiatry* **68**, 17 (Jul 1, 2010).
S10. J. L. McClelland, B. L. McNaughton, R. C. O'Reilly, *Psychol Rev* **102**, 419 (Jul, 1995).
S11. B. J. Wiltgen *et al.*, *Curr Biol* **20**, 1336 (Aug 10, 2010).
S12. J. B. Aimone, W. Deng, F. H. Gage, *Neuron* **70**, 589 (May 26, 2011).